International Journal of Mechanical, Industrial and Aerospace Sciences
ISSN: 2517-9950
Vol:12, No:9, 2018

Aerodynamic Performance of a Pitching Bio-Inspired Corrugated Airfoil

Hadi Zarafshani, Shidvash Vakilipour, Shahin Teimori, Sara Barati

Abstract**—**In the present study, the aerodynamic performance of a rigid two-dimensional pitching bio-inspired corrugate airfoil was numerically investigated at Reynolds number of 14000. The Open Field Operations And Manipulations (OpenFOAM) computational fluid dynamic tool is used to solve flow governing equations numerically. The k-ω SST turbulence model with low Reynolds correction (k-ω SST LRC) and the pimpleDyMFOAM solver are utilized to simulate the flow field around pitching bio-airfoil. The lift and drag coefficients of the airfoil are calculated at reduced frequencies k=1.24-4.96 and the angular amplitude of A=5°-20°. Results show that in a fixed reduced frequency, the absolute value of the sectional lift and drag coefficients increase with increasing pitching amplitude. In a fixed angular amplitude, the absolute value of the lift and drag coefficients increase as the pitching reduced frequency increases.

Keywords**—**Bio-inspired pitching airfoils, OpenFOAM, low Reynolds *k-ω SST* model, lift and drag coefficients.

I. Introduction

THE flight of insects, especially dragonflies, has fascinated scientists for more than a century to use their flight mechanism for designing airfoils with better aerodynamic performance [1]. The insects have single or tandem wing configurations. The corrugated, tandem configuration and flapping wings are the main origins of the high aerodynamic efficiency of insects [2].

In order to clarify the mechanism of insect generating force, Srygley and Thomas [3] performed experiments to investigate the lift generation mechanisms of butterfly in free-flying maneuver. They observed that these mechanisms are composed of: wake capture, active and inactive upstrokes, different types of leading-edge vortices, and rotation and 'clap and fling' movements. Ellington et al. [4] carried out visualizations of airflow around the wings of the hawkmoth *Manduca sexta*. They found out that the leading-edge vortex formed during the downstroke is the source of high lift forces.

The flight of dragonfly is also of interest of researchers to study its mechanisms and performance. Dragonflies have tandem corrugated wing configuration and fly at Reynolds number lower than 15000 [5]. They take-off with in-phase wing flapping and utilizes out of phase flapping in forward flight [6]. In-phase flapping produces high aerodynamic forces, and on the other hand, flapping out of phase results in better flight efficiency [7]-[9]

Tamai et al. [10] investigated the flow characteristics around corrugated and smooth airfoils at Reynolds number of 34000. Their experiments showed that the performance of the corrugated airfoil is superior in preventing stall as compared to the smooth one. Elie and Leavy [11] compared aerodynamic forces of a simplified corrugated dragonfly wing section with an Eppler-E61 airfoil at fixed angles of attack. They showed that the aerodynamic performance of the corrugated airfoil is better than the Eppler-E61 airfoil. Kwok and Mittal [12] investigated experimentally the aerodynamic performance of corrugated and smooth airfoils. They indicated that the lift coefficients of smooth and corrugated airfoils are nearly same. Murphy and Hu [13] performed measurements to compare the aerodynamic performance of a bio-inspired corrugate airfoil with a flat plate at Reynolds numbers of 58000-125000. They revealed that the lift and drag coefficients of the corrugated bio-airfoil are higher than those of flat plate. Harbig et al. [14] numerically investigated the effect of wing camber on flow structures and aerodynamic force for insect-like wings. They indicated that camber of the wing improved the aerodynamic performance and beneficial for flapping and rotating wing at Reynolds number smaller than 1500. Harbig et al [15] studied numerically the effect of wing aspect ratio (AR) and flow Reynolds number on flow structures over a bio-inspired wing. Their simulations showed that increasing of Reynolds number for an AR of 2.91 and increasing the AR at fixed Reynolds numbers between 120 and 1500 have the same effects on flow structures and increases the lift coefficient. Hord and Lian [16] performed structural simulation tests on the corrugate airfoil and flat plate. They showed that in the same thickness and weight of the airfoil, the resistance to bending moment of a corrugated airfoil is more than a flat plate. Flint and Jermy [17] studied the aerodynamic performance of a pitching bio-inspired corrugate airfoil and explained the characteristics of viscous flow formed around the corrugated airfoil. They showed that the corrugated airfoil produces thrust force at reduced frequency of 4.96 and angular amplitude of 20°.

In general, the surface topography of insect wings and their sections (bio-airfoils) are corrugated and irregular. Moreover, the vortices formed inside the bio-airfoil surface cavities play an important role in wakes and turbulence flow structures around and behind of them during flapping process, especially, at Reynolds numbers above 10000. Therefore, to study the aerodynamic characteristics of a bio-airfoil at high

Hadi Zarafshani is with the Department of Aerospace Engineering, Faculty of New Sciences and Technologies, University of Tehran, Tehran, Iran (e-mail: zarafshani.hadi@ut.ac.ir).

Shidvash Vakilipour is with the Department of Aerospace Engineering, Faculty of New Sciences and Technologies, University of Tehran, Tehran, Iran (phone: +989121326951, e-mail: vakilipour@ut.ac.ir).

Shahin Teimori is with the Shahid Beheshti University, Iran (e-mail: steimori1950@gmail.com).

Sara Barat is with the Department of Chemistry, Islamic Azad University, Iran (e-mail: sarabarati1973@gmail.com).

Reynolds numbers, it is indispensable to use appropriate turbulence models to resolve flow structures at the vicinity of a bio-airfoil surface. The main objective of the present study is to resolve the near surface flow structures of a corrugated pitching airfoil by utilizing the k-ω SST turbulence model with low Reynolds number corrections (k-ω SST LRC). This model accommodates the transitional process and its numerical results are in good agreement with those of experiments [18]. In this regard, the flow field around a pitching bio-inspired airfoil at Reynolds number of 14000 is numerically solved to describe its unsteady aerodynamic characteristics influenced by pitching parameters.

II. Numerical Modeling

The flow field around the pitching corrugated airfoil can be modeled by the unsteady incompressible of continuity and Navier-Stokes equations. Written in primitive-Variables these equations are as follows:

$$\nabla.\vec{V} = 0 \tag{1}$$

$$\frac{\partial \vec{V}}{\partial t} + (\vec{V}.\nabla)\vec{V} = -\frac{\nabla p}{\rho} + \nu\nabla^2\vec{V} \tag{2}$$

where $\vec{V}(u,v,w)$, p, ρ and ν are the flow velocity, pressure, density, and fluid kinematic viscosity, respectively.

In this study, a rigid two-dimensional bio-inspired corrugated airfoil was modeled using OpenFOAM version 3.0.1. OpenFOAM is an open source collection of numerical solvers and utilities [19]. Lift and drag coefficients of a pitching airfoil are calculated at constant Reynolds number (Re) of 14000, reduced frequencies (k) between 1.24 and 4.96, and angular amplitude (A) between 5° and 20°. It is worth mentioning that the pitching axis is at the quarter-chord of the airfoil.

$$Re = \frac{Uc}{\nu} \tag{3}$$

$$k = \frac{\pi\, fc}{U} \tag{4}$$

where U, c, and f are the free stream velocity, airfoil chord length, and frequency of oscillation, respectively. Details of the airfoil geometry numerically studied in the present work was described by Flint and Jermy [17]

The pitching process of corrugated airfoil is modeled by the sliding mesh technique of OpenFOAM using Arbitrary Mesh Interface (AMI). Fig. 1 illustrates and the grid far from the airfoil Fig. 1 (a), the airfoil section Fig. 1 (b), and the details of grid near the airfoil surface Fig. 1 (c). The flow domain shown in Fig. 1 (a) consists of two subdomains: outer (stationary) and inner (pitching) domain separated by a sliding surface. The grid resolution in viscous flow boundary layer is generated by quadrilateral cells where the maximum y^+ kept below 1 for near wall calculations of used turbulence model.

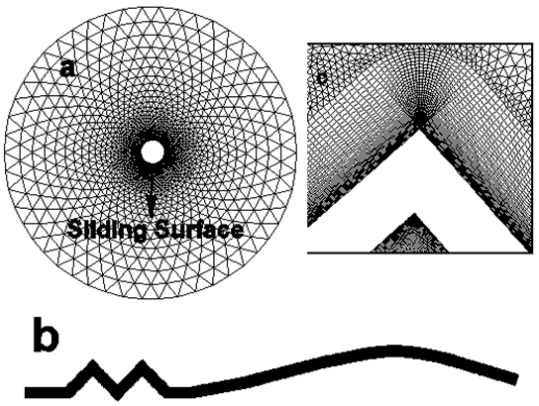

Fig. 1 Problem solution field: a) Outer boundary, b) airfoil section, c) boundary layer quadrilateral cells

The implemented boundary conditions on the outer boundary of stationary domain are inletOutlet for velocity and outletInlet for pressure fields. The no-slip velocity and zeroGradient condition for the pressure are imposed at the airfoil surface. The cyclicAMI conditions are implemented for sliding surface between inner and outer domain. The pimpleDyMFoam solver was used to solve the current unsteady moving boundary problem. The first order and second order discretization schemes are used to discretize time and space derivatives, respectively.

III. Results and Discussion

A. Courant Number

In an implicit algorithm, the requirement of setting the Courant number (C) threshold is essentially enforced by the relative propagation of the physical and numerical solution information. The Courant number in a computational cell is defined as:

$$C = \frac{U\,\Delta t}{\Delta h_m} \tag{5}$$

where Δt is the simulation time-step and Δh_m is the minimum height (characteristic length) of the grid cells. In the present study, stable numerical solutions were achieved by C≤2.5, and all simulations have been carried out by the most possible value for Courant number.

The lift and drag coefficients, C_L and C_D, are computed using the following formulas:

$$C_L = \frac{\boldsymbol{f}.e_y}{\frac{1}{2}\rho U^2 c} \tag{6}$$

$$C_D = \frac{\boldsymbol{f}.e_x}{\frac{1}{2}\rho U^2 c} \tag{7}$$

where $\boldsymbol{f}$ is the total fluid flow force and defined as:

$$\boldsymbol{f} = \int_{\Gamma} (-pI + \tau).\hat{\boldsymbol{n}} dA \tag{8}$$

In (6)-(8), e_x, e_y, Γ, τ, I, $\hat{\boldsymbol{n}}$, and A are the unit vectors in the x and y coordinate directions, boundary of the airfoil, stress tensor, identity matrix, outer unit normal vector to the boundary, and surface element of the airfoil, respectively.

Pressure Coefficient (C_p) is calculated from the following equation:

$$C_p = \frac{P - P_\infty}{\frac{1}{2}\rho U^2} \tag{9}$$

where P and P_∞ are the pressure at point of interest and the pressure at the far field, respectively.

B. Comparison of Turbulence Models

As was mentioned before, the aerodynamic characteristic of current pitching bio-airfoil is determined by the different interactions of moving vortices generated from the corrugated oscillating airfoil surface. Therefore, it is necessary to use proper turbulence model to resolve different scales of flow structures and predict their influences on the aerodynamic performance. In this work, the k-ω SST LRC is implemented on the OpenFOAM 3.0.1 platform to model the turbulent flow field in all simulations [20]. In order to verify the present numerical results, they are compared with those obtained by k-ω SST SAS.

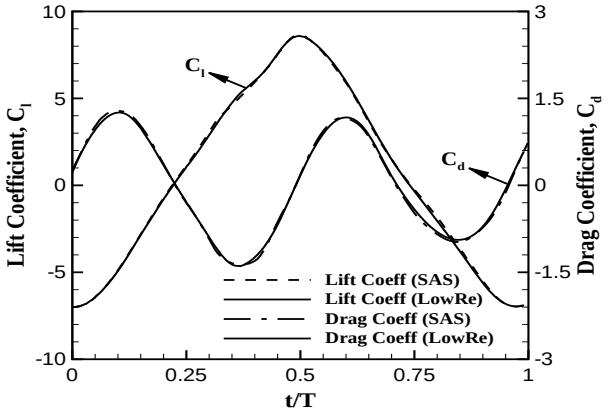

Fig. 2 The lift and drag coefficients (C_l and C_d) during one cycle of corrugated pitching bio-airfoil calculated from k-ω SST LRC and SAS turbulence modeling

Fig. 2 illustrates the predicted aerodynamic force coefficients (C_l and C_d) in a cycling period of pitching bio-airfoil. The numerical results are obtained using k-ω SST LRC (present) and k-ω SST SAS turbulence models. The simulations are performed at reduced frequency of k=2.48 and the pitching amplitude of A=20°. As is seen in Fig. 2, both utilized turbulence models result in same aerodynamic force on the corrugated bio-airfoil. Therefore, the k-ω SST LRC turbulence model accomplishes equivalent pressure and viscous forces with those of k-ω SST SAS on present corrugated airfoil section.

C. The Grid Independence of Solution

In order to investigate the effects of mesh resolution on the numerical results, the flow computations are performed on three meshes with about 35k, 65k, and 95k cells. The reduced frequency and pitching amplitude are 4.96 and 20°, respectively. Fig. 3 demonstrates the calculated lift coefficient, C_l, during a period of pitching cycle on three grid resolutions. The most significant effects of grid resolution on the C_l are estimated at the highest absolute values of lift coefficient; i.e. at t/T=0.25 and 0.75. Moreover, Fig. 3 indicates that the grid with 35k cells has lower accuracy compared to grids with 65k and 95k cells. On the other hand, the numerical results carried out from the flow computations on grids with 65k and 95k cells are acceptably close to each other. Thus, the mesh with 65k cells is used for the rest of flow simulations throughout the present study.

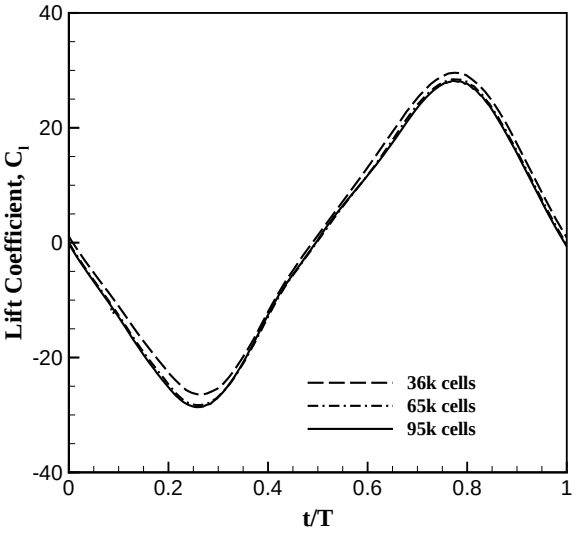

Fig. 3 Lift coefficient calculated on different grid resolutions at k=4.96 and A=20°

D. Verification

Fig. 4 shows the lift and drag coefficients predicted for the flow around pitching airfoil with k=2.48 and A=20°. The numerical results of Flint et al. [17]. The comparison between lift and drag coefficients presented in Fig. 4 shows that the present numerical approximations match accurately with those of [17].

E. Surface Pressure and Flow Characteristics

Although the total aerodynamic force exerted on the flapping wings is a result of pressure and stress (shear and normal) forces, its most portion consists of pressure force at relatively low Reynolds and high angles of attack. In order to

assess the pressure force acting on the pitching bio-airfoil, the upper and lower surface distribution of pressure coefficient in upstroke and downstroke is demonstrated in Figs. 5 (a) and (b), respectively.

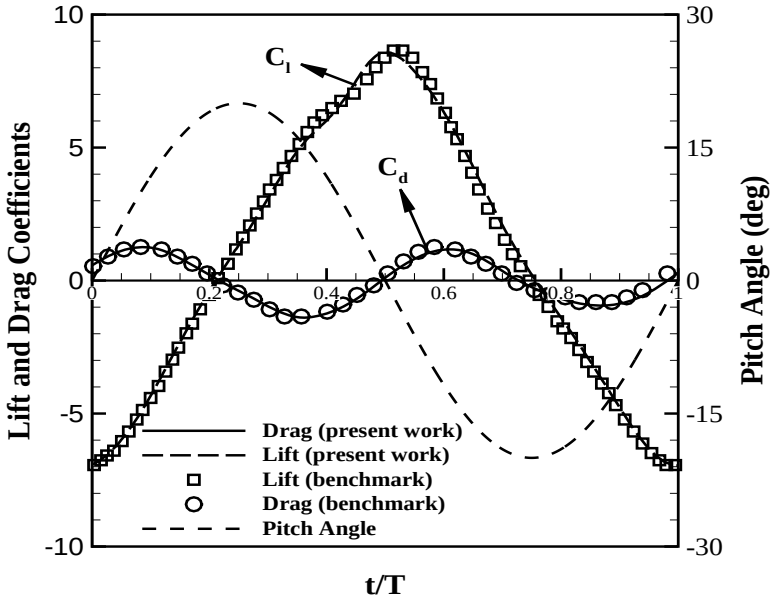

Fig. 4 Comparison the Lift and Drag Coefficients of present work with benchmark [17] for k=2.48, A=20°

The pressure coefficient is computed for the airfoil at zero angle of attack. In upstroke, the net pressure force is negative, i.e. the bio-airfoil experiences a downward (negative lift) force. Also, the absolute value of the negative lift force on the curved portion of bio-airfoil is significantly higher than its value on the corrugated part. On the other hand, in downstroke, the bio-airfoil yields positive lift force and its most value is exerted on the curved portion of airfoil.

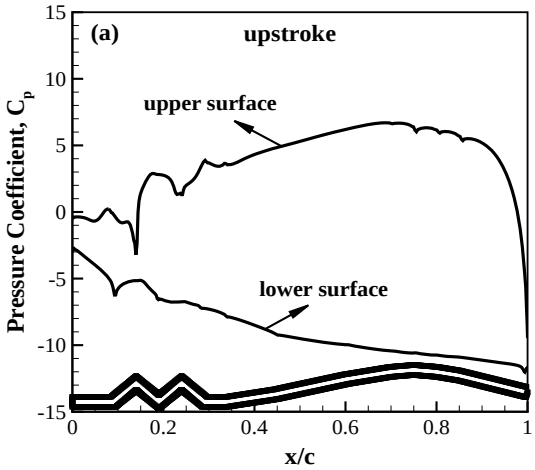

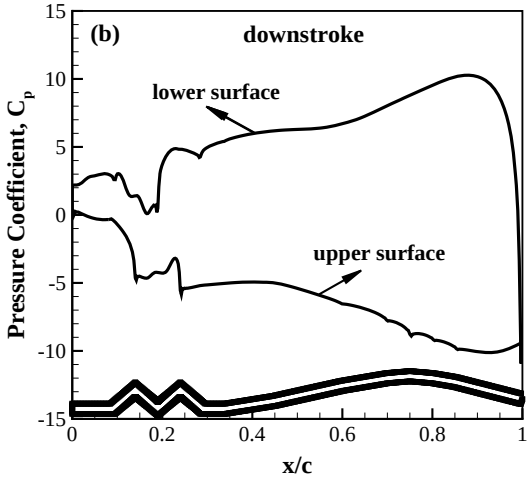

Fig. 5 Pressure coefficient on the upper and lower surface of bio-airfoil in upstroke (a) and downstroke (b) at zero angle of attack and k=4.96, A=20°

Figs. 6 (a) and (b) depicts the streamlines of flow field around pitching bio-airfoil at upstroke and downstroke, respectively. The formation and shedding of the vortices around the pitching airfoil play important role on the lift and drag production during upstroke and downstroke. In upstroke, a strong vortex placed on the aft-end top of the airfoil where a relatively high pressure region is generated in upstroke maneuver. This aft-end vortex is responsible for pressurizing flow above the curved part of airfoil, and consequently the

negative lift at zero angle of attack in upstroke. Moreover, there is a relatively weak vortex under the first quarter part of vortex. As is seen, the flow direction within the vortex generates low pressure (suction) region under this part of bio-airfoil in upstroke. In downstroke (see Fig. 6 (b)), a vortex is formed under aft-end of airfoil which makes the pressure grows up under curved portion of bio-airfoil. Also, the vortices predicted above the first quarter of the airfoil play a role for the high pressure region on that part, and then, a positive lift force is exerted on the airfoil at zero angle of attack.

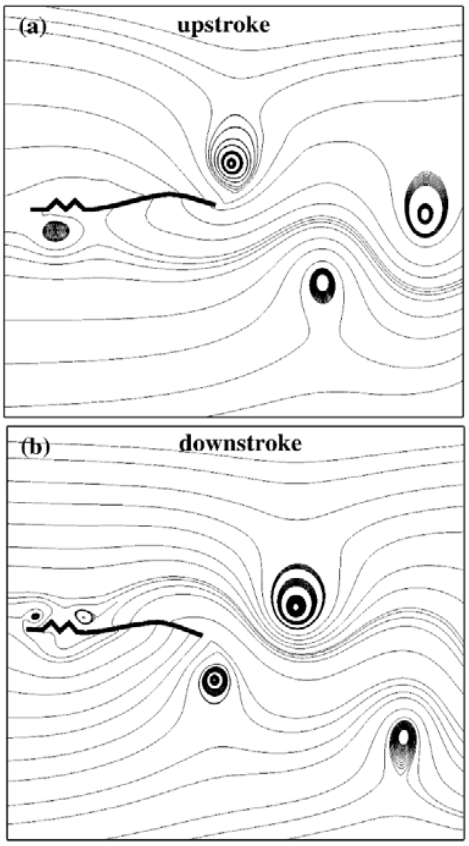

Fig. 6 Flow field streamlines and predicted vortices around pitching bio-airfoil in upstroke (a) and downstroke (b) at k=4.96, A=20°

F. Effects of Reduced Frequency and Angular Amplitude

In this section, the effects of reduced frequency and angular amplitude on the lift and drag coefficient of pitching bio airfoil are investigated. Fig. 7 demonstrates the dynamic hysteresis in lift coefficient estimated at different reduced frequencies and pitching amplitudes. As expected, at fixed reduced frequency, increasing oscillation amplitude results in increments in absolute value of C_l. In addition, the increment in reduced frequency increases C_l by keeping angular amplitude constant. The angles of attack where the extrema of C_l are obtained are the other parameters which could be studied considering the hysteresis in Fig. 7. As is seen, the angles of attack corresponding to the maximum and minimum C_l at k=1.24 are A=-7° and +7°, respectively. At k=1.24, the maximum and minimum C_l are predicted to be at A=0°. Finally, at the highest reduced frequency, i.e. k=4.96, the maximum and minimum C_l are estimated at A=+7° and -7°, respectively. Therefore, the increments of pitch reduced frequency have influence on the generation and shedding of flow vortices in which the maximum lift produced at higher angles of attack.

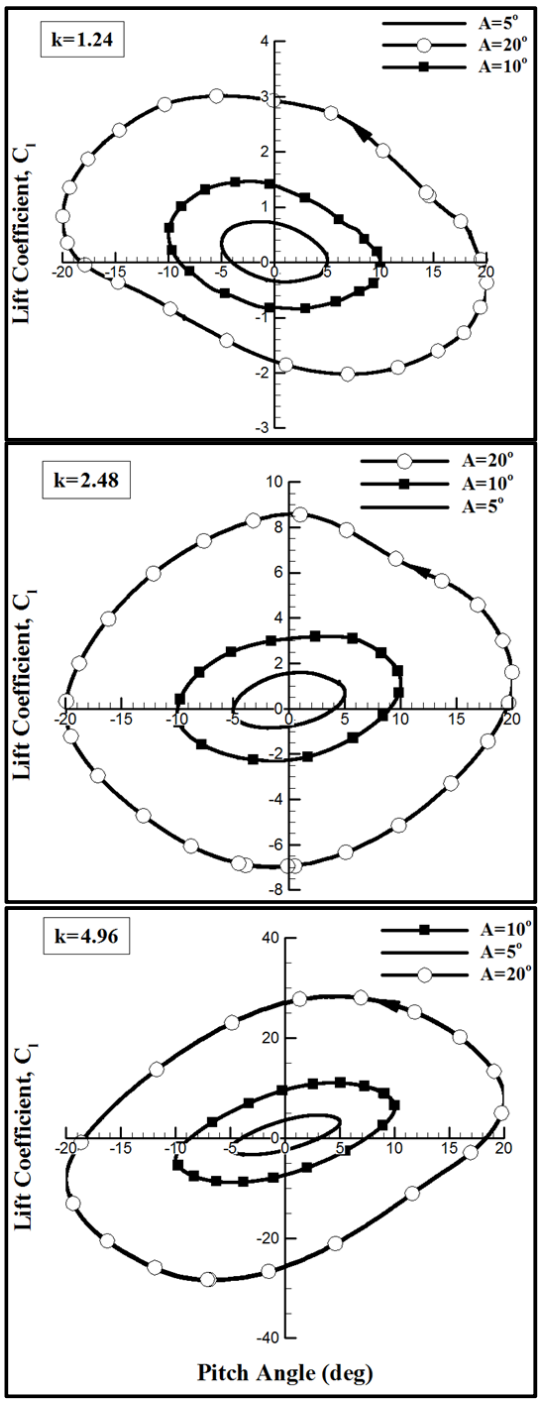

Fig. 7 Estimated dynamic hysteresis in the lift coefficient of pitching bio-airfoil at three values of k and A

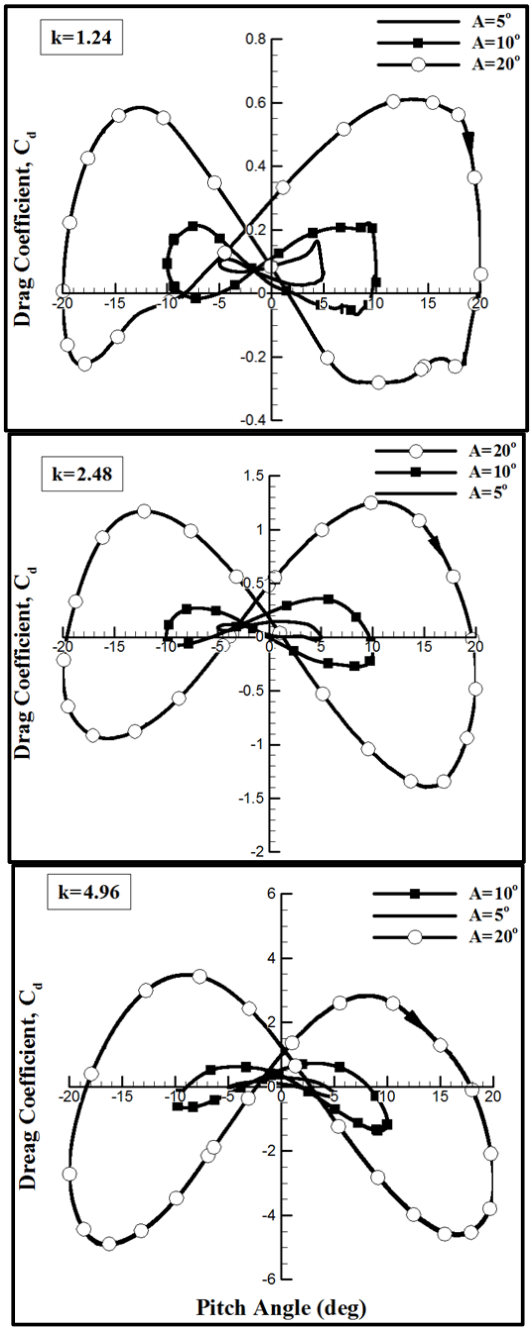

Fig. 8 Estimated dynamic hysteresis in the drag coefficient of pitching bio-airfoil at three values of reduced frequency, k, and angular amplitude, A

Fig. 8 illustrates the dynamic hysteresis in drag coefficient estimated at different reduced frequencies and pitching amplitudes. The influences of increasing of reduced frequency and angular amplitude on C_d are similar to what they do on C_l. The main outcome revealed from Fig. 8 plots is the effects of change of reduced frequency and pitching amplitude on the propulsion performance of pitching bio-airfoil. As is observed, as the angular amplitude increases, there is an ability for producing propulsive force even at low reduced frequency. The propulsive force takes place at negative and positive angles of attack during upstroke and downstroke, respectively. Increasing the pitching reduced frequency results in large propulsive force and wider range of propulsive angles of attack.

IV. Conclusion

Flow around a pitching bio-inspired corrugate airfoil undergoing a pitching motion was modeled using OpenFoam computational fluid dynamics tool utilizing low Reynolds k-ω SST turbulence model. The aerodynamic coefficients were calculated at constant Reynolds number of 14000, reduced frequency, k, and angular amplitude, A, ranging from between 1.24-4.96 and 5°-20°, respectively.

In this regard, the main conclusions are as follows:

1. The aft-end section of the airfoil produces the most amount of the lift force,
2. In a fixed reduced frequency, absolute value of the sectional lift and drag coefficients increase with increasing oscillation amplitude,
3. In a fixed angular amplitude, absolute value of the sectional lift and drag coefficients increase with increasing oscillation reduced frequency,
4. The pitching bio-airfoil is able to produce propulsive force at sufficient high angular amplitude.

References

[1] S. P. Sane, "The aerodynamics of insect flight," *Journal of experimental biology,* vol. 206, no. 23, pp. 4191-4208, 2003.
[2] W. Shyy *et al.*, "Computational aerodynamics of low Reynolds number plunging, pitching and flexible wings for MAV applications," *Acta Mechanica Sinica,* vol. 24, no. 4, pp. 351-373, 2008.
[3] R. Srygley and A. Thomas, "Unconventional lift-generating mechanisms in free-flying butterflies," *Nature,* vol. 420, no. 6916, pp. 660-664, 2002.
[4] C. P. Ellington, C. Van Den Berg, A. P. Willmott, and A. L. Thomas, "Leading-edge vortices in insect flight," *Nature,* vol. 384, no. 6610, pp. 626-630, 1996.
[5] B. Newman, "Model tests on a wing section of an Aeschna dragonfly," *Scale Effects in Animal Locomotion,* 1977.
[6] D. E. Alexander, "Unusual phase relationships between the forewings and hindwings in flying dragonflies," *Journal of Experimental Biology,* vol. 109, no. 1, pp. 379-383, 1984.
[7] G. Rüppell, "Kinematic analysis of symmetrical flight manoeuvres of Odonata," *Journal of Experimental Biology,* vol. 144, no. 1, pp. 13-42, 1989.
[8] A. Azuma and T. Watanabe, "Flight performance of a dragonfly," *Journal of Experimental Biology,* vol. 137, no. 1, pp. 221-252, 1988.
[9] A. L. Thomas, G. K. Taylor, R. B. Srygley, R. L. Nudds, and R. J. Bomphrey, "Dragonfly flight: free-flight and tethered flow visualizations reveal a diverse array of unsteady lift-generating mechanisms, controlled primarily via angle of attack," *Journal of Experimental Biology,* vol. 207, no. 24, pp. 4299-4323, 2004.
[10] M. Tamai, Z. Wang, G. Rajagopalan, H. Hu, and G. He, "Aerodynamic performance of a corrugated dragonfly airfoil compared with smooth airfoils at low Reynolds numbers," in *45th AIAA Aerospace Sciences Meeting and Exhibit*, 2007, pp. 1-12.
[11] D.-E. Levy and A. Seifert, "Simplified dragonfly airfoil aerodynamics at Reynolds numbers below 8000," *Physics of Fluids,* vol. 21, no. 7, p. 071901, 2009.
[12] M. Kwok and R. Mittal, "Experimental investigation of the aerodynamics of a modeled dragonfly wing section," in *AIAA region I-MA Student Conference, Charlottesville, Virginia April*, 2005, pp. 8-9.
[13] J. T. Murphy and H. Hu, "An experimental study of a bio-inspired corrugated airfoil for micro air vehicle applications," *Experiments in*

fluids, vol. 49, no. 2, pp. 531-546, 2010.
[14] R. Harbig, J. Sheridan, and M. Thompson, "Relationship between aerodynamic forces, flow structures and wing camber for rotating insect wing planforms,"*Journal of Fluid Mechanics,* vol. 730, pp. 52-75, 2013.
[15] R. Harbig, J. Sheridan, and M. Thompson, "Reynolds number and aspect ratio effects on the leading-edge vortex for rotating insect wing planforms," *Journal of Fluid Mechanics,* vol. 717, pp. 166-192, 2013.
[16] K. Hord and Y. Lian, "Numerical investigation of the aerodynamic and structural characteristics of a corrugated airfoil," *Journal of Aircraft,* vol. 49, no. 3, pp. 749-757, 2012.
[17] T. Flint, M. Jermy, T. New, and W. Ho, "Computational study of a pitching bio-inspired corrugated airfoil," *International Journal of Heat and Fluid Flow,* vol. 65, pp. 328-341, 2017.
[18] M. Seyednia, S. Vakilipour, and M. Masdari, "Numerical Investigation of Dynamic Stall over a Wind Turbine Pitching Airfoil by Using OpenFOAM," *World Academy of Science, Engineering and Technology, International Journal of Mechanical, Aerospace, Industrial, Mechatronic and Manufacturing Engineering,* vol. 11, no. 8, pp. 1466-1477, 2017.
[19] URL http://www.openfoam.org.
[20] URL http://www.cfd-online.com/Forums/openfoam-programming-development/134102-komegasst-lowre-damping-fluent.html.